Computational modeling of pharmacokinetics and tumor dynamics to guide anti-cancer treatment

Yin, A.

Chapter 4

Quantitative modeling of tumor dynamics and development of drug resistance in non-small cell lung cancer patients treated with erlotinib

Anyue Yin, G.D. Marijn Veerman, Johan G.C. van Hasselt, Christi M.J. Steendam, Hendrikus Jan Dubbink, Henk-Jan Guchelaar, Lena E. Friberg, Anne-Marie C. Dingemans, Ron H.J. Mathijssen, Dirk Jan A.R. Moes

Submitted

Abstract

Insight into the development of treatment resistance can support the optimization of anti-cancer treatments. This study aims to characterize the tumor dynamics and development of drug resistance in non-small cell lung cancer (NSCLC) patients treated with erlotinib, and investigate the relationship between baseline circulating tumor DNA (ctDNA) data and tumor dynamics. Data obtained for the analysis included 1) intensively sampled erlotinib concentrations from 29 patients from two previous pharmacokinetic (PK) studies, and 2) tumor sizes, ctDNA measurements, and sparsely sampled erlotinib concentrations from 18 patients from the START-TKI study. A two-compartment population PK model was first developed which well described the PK data. The PK model was subsequently applied to investigate the exposure-tumor dynamics relationship. To characterize the tumor dynamics, models accounting for intra-tumor heterogeneity and acquired resistance with or without primary resistance were investigated. Eventually, the model assumed acquired resistance only resulted in an adequate fit. Additionally, models with or without exposure-dependent treatment effect were explored, and no significant exposure-response relationship for erlotinib was identified within the observed exposure range. Subsequently, the correlation of baseline ctDNA data on *EGFR* and *TP53* variants with tumor dynamics parameters was explored. The analysis indicated that higher baseline plasma *EGFR* mutation levels correlated with increased tumor growth rates, and the inclusion of ctDNA measurements improved model fit. This result suggests that quantitative ctDNA measurements at baseline have the potential to be a predictor of anti-cancer treatment response. The developed model can potentially be applied to design optimal treatment regimens that better overcome resistance.

Keywords: oncology, quantitative modeling, intra-tumor heterogeneity, tumor dynamics, resistance development, non-small cell lung cancer, circulating tumor DNA

1. Introduction

The occurrence of anticancer treatment resistance due to intra-tumor heterogeneity and evolving adaptation of tumor cells to the treatment can limit the long-lasting efficacy of targeted anticancer treatment [1, 2]. In order to improve the anti-cancer treatment outcome, it is important to have detailed insight into the tumor progression during treatment since it enables designing of alternative treatment strategies.

In patients with non-small cell lung cancer (NSCLC), erlotinib, a tyrosine kinase inhibitor (TKI), is one of the effective treatment options especially for patients with *EGFR* exon 19 deletions or exon 21 mutations [3-5]. However, the occurrence of acquired drug resistance, which is most frequently due to the acquisition of the *EGFR* p.T790M mutation, and the possible presence of drug-resistant component pre-treatment (primary resistance) can limit its efficacy and result in relapse [3-6]. Thus, understanding the evolving progression of NSCLC during the treatment and identifying predictive biomarkers would be beneficial to optimize the treatment of NSCLC.

Pharmacometric modeling allows quantitative characterization and prediction of pharmacokinetic (PK) – pharmacodynamic (PD) profiles of drugs and thus facilitates treatment design [7-9]. With the help of a model-based approach, studies on evolving tumor progression can be conducted based on available data on tumor sizes and genetic biomarkers, and optimal treatment designs can be evaluated. Our previous study has proven such a concept based on data from metastatic colorectal cancer patients as well as from NSCLC patients [10]. Further incorporating the exposure of therapeutic agents in the model can support the investigation and understanding of exposure-tumor inhibition relationship and the evolutionary tumor dynamics in relation to drug exposure during anti-cancer treatment.

Circulating tumor DNA (ctDNA), which are DNA fragments in the circulation (circulating free DNA (cfDNA)) that are of tumor origin, is a clinically available and emerging genetic biomarker [11]. It has shown to be able to provide detailed insight into the molecular alterations and evolving progression of tumor under treatment [4, 5, 11]. In patients with NSCLC, numerous studies have shown that a decrease in mutant gene levels in ctDNA correlates to the therapeutic response of TKIs [5]. In another model-based study, the relative change of concentrations of driver mutation in ctDNA from the estimated baseline was shown to be predictive to disease progression of NSCLC patients [12]. Further research on the correlation between ctDNA measurements and tumor size dynamics would be beneficial to understanding the evolutionary development of treatment resistance and the value of ctDNA.

In the current study, we aimed to develop a model to understand and characterize tumor dynamics and the development of drug resistance in NSCLC patients treated with erlotinib. First, a population PK model of erlotinib was developed and thereafter applied to investigate the exposure-tumor inhibition relationship of erlotinib. Tumor dynamics models accounting for tumor heterogeneity, with or without a pre-existing resistance component, and drug exposure-dependent treatment effects, were evaluated. Subsequently, we aimed to explore the correlation of the extent of somatic driver mutation in ctDNA at baseline with the tumor dynamics in NSCLC patients.

2. Method

2.1 Patients and data

2.1.1 Intensively sampled PK data

The study included intensively sampled erlotinib concentration-time curves from two previous PK studies in patients with NSCLC who were treated with erlotinib for an activating EGFR mutation [13, 14]. Erlotinib was administrated orally once daily with a dosage of 50–150 mg. PK samples were collected before drug intake and at 0.5, 1, 1.5, 2, 2.5, 3, 3.5, 4, 6, 8, 12, and 24 hours after drug administration at steady state. The studies were performed at the Erasmus MC Cancer Institute in Rotterdam, the Netherlands, and the details of the studies' design can be found in previous publications [13, 14]. For the current study, only the data in the control arms that were sampled after receiving erlotinib with water and without concomitant esomeprazole were included, which aimed to be consistent with real world patients.

Patients' demographic information, including age, sex, weight, height, and additional laboratory test results, including creatinine, estimated glomerular filtration rate (eGFR), albumin, total bilirubin, aspartate aminotransferase (AST), alanine aminotransferase (ALT), and alkaline phosphatase (ALP) were collected for covariate analysis.

2.1.2 PK-PD data

Longitudinal measured tumor sizes under standard clinical care conditions as well as sparsely sampled intended trough erlotinib concentrations from real-world NSCLC patients who participated in the START-TKI study (NCT05221372), which is a prospective, observational multicenter study [6], were also included in this analysis. Erlotinib was administrated orally once daily with a dosage of 75–150 mg. The tumor size measurements,

i.e. the sum of the longest diameters (SLD, mm) of target lesions, were assessed by Response Evaluation Criteria In Solid Tumors (RECIST version 1.1 [15]). Additional data of dosing information, ctDNA data on variant allele frequency (VAF) of mutant genes over time, and concentrations of cfDNA over time from these patients were also collected. The detailed methods of cfDNA isolation and next-generation sequencing process have earlier been described [6]. Patients demographic information and lab test results as above mentioned were also collected for potential covariate analysis.

The studies from which the data were obtained were previously approved by local ethics committee and were registered in the Dutch Trial Registry. Written informed consent was obtained from all patients prior to these studies, including the use of data for further studies. For the current study, the data were shared anonymously and all procedures were performed in accordance with relevant guidelines and the Declaration of Helsinki, so no additional informed consent had to be obtained.

2.2 Population PK model

Based on the collected PK data, a population PK model was developed to characterize the erlotinib PK profiles of included patients. The intensively sampled PK data and the sparsely sampled PK data from patients involved in the START-TKI study were combined for the model development.

One- and two-compartment models with first-order absorption, with or without lag time, and first-order elimination were explored as the structural model. A combined proportional and additive model was applied to characterize the residual error. Parameters were assumed to be log-normally distributed. To account for the inter-individual variability (IIV) in bioavailability (F) which is shared by the estimated apparent PK parameters, the IIV on F was estimated while the typical value of F was fixed to 1. The structural model was selected based on biological plausibility and the objective function value (OFV).

Patients' demographic information and lab test results were then investigated as covariates using the stepwise covariate modeling (SCM) function of Perl-speaks NONMEM (version 4.9). The effect of all covariates on erlotinib clearance and that of weight, height, and albumin on apparent distribution volume of the central compartment were investigated. The relationship between F and dose level was not explored since the majority of patients received the same dose level. Model selection was based on the reduction in OFV (a likelihood ratio test) assuming a χ^2 distribution, a reduction in IIV, and physiological plausibility. The p values were set as 0.05 and 0.01 for the forward selection and backward

elimination process, respectively. A more detailed description of the covariates analysis can be found in **Supplementary Material S4.1**.

The final model was evaluated with goodness-of-fit (GOF) plots, visual predictive checks (VPC) based on 1000 simulations, and bootstrap with 1000 resampled datasets. In addition, the percentage where the predicted area under the curve (AUC) falls within 80–120% of the corresponding observed AUC (estimated with trapezoidal rules method) was calculated for the full concentration-time curves to evaluate the model. The percentage where the predicted trough concentrations fall within 80–120% of the corresponding observations was also estimated for the data from the START-TKI study.

2.3 Tumor dynamics model

The dynamics of tumor sizes during erlotinib treatment, which was represented by sum of longest diameters (SLD, mm) of target lesions, was characterized accounting for tumor heterogeneity. Tumor tissue was assumed to consist of a sensitive clonal population (T_s) and a resistant clonal population (T_R). Models considering 1) only acquired resistance and no primary resistance (i.e. baseline T_R (T_{R_0}) = 0), and 2) both primary and acquired resistance (i.e. $T_{R\_0} \neq 0$ and was estimated), with or without a drug exposure-dependent decay, were explored. Considering the amount of the available data, the baseline tumor sizes were fixed to the observed values to ensure the stability of the model. The model structure is shown in **Figure 4.1** and Eqs. 4.1–4.4, where k_g represents the growth rates of T_s and T_R, k_m represents mutation rate, and k_d represents tumor decay rate due to treatment. For the models exploring the exposure-dependent treatment effect, the tumor decay rate was assumed to depend on drug exposure and a simple linear relationship was assumed (Eq. 4.2). A non-linear relationship with Emax model was also explored. The drug exposure was defined as the trough concentration, which is the exposure metrics of interest for erlotinib exposure-response analysis and is relatively easy to measure in clinical practice. The trough concentrations were predicted by the individual PK parameters obtained from the PK model. The IIV of parameters were evaluated and parameters were assumed to be log-normally distributed. The combined proportional and additive model was applied to

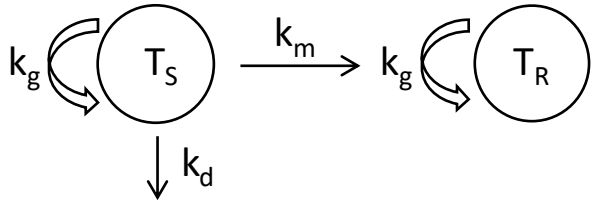

Figure 4.1: Graphical structure of the tumor dynamics model.

characterize the residual error. The model fit was evaluated by OFV and Akaike information criterion (AIC). The best fitted model was evaluated with GOF plots and VPC considering the censoring of data due to progression defined by RECIST version 1.1 [15].

$$\frac{dT_S}{dt} = k_g \cdot T_S - k_d \cdot T_S - k_m \cdot T_S \quad \text{Eq. 4.1}$$

$$k_d = \begin{cases} k_d, & for\ the\ model\ without\ exposure - dependent\ decay \\ k_d \cdot Exposure, & for\ the\ model\ with\ exposure - dependent\ decay \end{cases} \quad \text{Eq. 4.2}$$

$$\frac{dT_R}{dt} = k_m \cdot T_S + k_g \cdot T_R \quad \text{Eq. 4.3}$$

$$TS = T_S + T_R \quad \text{Eq. 4.4}$$

2.4 Genetic biomarkers and tumor dynamics

The correlation of baseline ctDNA measurements, including *EGFR* mutation levels and the presence of *TP53* mutations, with tumor dynamics parameters (k_g, k_m, and k_d) were explored graphically. Patients were separated into groups based on 1) whether their baseline mutant *EGFR* VAF was < or ≥ the median value, or the measurements were unavailable, or 2) whether patients had a *TP53* mutation at baseline or not, or the results were unavailable. The correlation between baseline cfDNA concentrations and tumor dynamics parameters was also explored by separating patients into groups based on the median value to investigate informativeness of cfDNA compared to ctDNA.

Furthermore, the influence of baseline ctDNA measurements and cfDNA concentrations on k_g, k_m, and k_d were evaluated as categorical covariates in the tumor dynamics model. The EGFR mutation levels and the cfDNA concentrations were categorized based on the corresponding median values as is described above. When a sample is missing, it was assigned to the third category and a sensitivity analysis was performed by evaluating models with and without the covariate for a dataset where the data from patients with missing covariates were removed. A significant correlation was defined as a decrease in OFV by more than 3.84 ($p < 0.05$, degree of freedom = 1, assuming χ^2 distribution).

2.5 Software and estimation methods

The population modeling analysis in this study was performed with NONMEM (version 7.4.4, ICON Development Solutions, Ellicott City, MD, USA). Parameters were estimated using the first order conditional estimation method with interaction (FOCEI). Data management and plots generation were performed with R statistics software (version 4.2.1, R Foundation for Statistical Computing, Vienna, Austria).

3. Results

3.1 Patients and data

The intensively sampled erlotinib concentration-time curves were obtained from 29 patients (N = 377, 13 samples per patient). The SLD measurements (N = 155) as well as additionally sampled erlotinib concentrations (N = 146), ctDNA measurements (N = 50), and cfDNA concentrations (N = 50) were collected from 18 real-world NSCLC patients from the START-TKI study. For these 18 patients, the median time period when the SLD measurements were available is 264 days since the start of the treatment (range from 20–1168 days), and all patients had an event of disease progression or death where data were censored afterwards.

The obtained erlotinib concentration data over time are presented in **Figure S4.1**. None of the collected data was below the lower limit of quantification. The median baseline tumor size (SLD) of the included patients was 76.6 mm (range 29–116 mm). Out of the 146 obtained concentrations, 125 were measured at ≥ 20 hours after last drug intake (trough concentrations) with a median of 842 ng/mL and range of 318–1834 ng/mL. Activating *EGFR* variants (including exon 19 deletions (N = 11) and *EGFR* p.L858R (N = 6) and p.K852R (N = 1) mutations) were detected in the tumor biopsies of all 18 patients [6]. The plasma cfDNA samples at the start of treatment were available from 12 out of 18 patients. The median baseline cfDNA concentration was 1.44 ng/μL (range from 0.77–3.65 ng/μL). The primary *EGFR* variants were detected from baseline cfDNA samples from 8 out of 12 patients, which include exon 19 deletions (N = 6) and *EGFR* p.L858R (N = 1) and p.K852R (N = 1) mutations. The median baseline *EGFR* VAF was 1.74% (range from 0–62.74%). The obtained VAF of primary EGFR variants over time are shown in **Figure S4.2**. Furthermore, a *TP53* mutation was detected in 4 patients at baseline and the *EGFR* p.T790M mutation was detected in 3 patients during erlotinib treatment. The baseline characteristics and the data contributed by each patient are summarized in **Table 4.1**.

3.2 Population PK model

A two-compartment population PK model with first-order absorption with lag time and first-order elimination was developed and showed to best fit the obtained PK data. Compared to the one-compartment model, the OFV of the selected model decreased by 27.5 ($p < 0.01$, degree of freedom = 3), indicating an improvement in the model fit. None of the tested covariates was identified to have significant effect on the PK parameters. The parameter estimates of the PK model are presented in **Table 4.2**. The relative standard errors (RSEs) were ≤ 25% for all parameters except for apparent distribution clearance

Table 4.1: Baseline characteristics of patients and the collected data

	Intensively sampled PK data (N = 29)		PK/PD data (N = 18)	
	Median	Range	Median	Range
Age (years)	63	35–78	66	48–78
Sex (N (%))				
Male	13 (44.8%)		5 (27.8%)	
Female	16 (55.2%)		13 (72.2%)	
Weight (kg)	74	50–102	69.5	46.1–109
Height (cm)	173	152–202	169	154–180
Serum creatinine (µmol/L)	82	47–138	66	59–192
eGFR (ml/(min.1.73 m^2))	71	46–100	84.5	23–103
AST (IU/L)	29	13–40	21.5	14–37
ALT (IU/L)	25	10–83	18	6–43
Albumin (g/L)	41	32–48	42.5	34–51
ALP (U/L)	85	53–157	87.5	3–798
Bilirubin (µmol/L)	8	3–58	6.5	3–14
Erlotinib starting dose (N (%))				
150 mg	25 (86.2%)		18 (100%)	
100 mg	3 (10.3%)		0	
50 mg	1 (3.4%)		0	
N of concentration per patient	13	13–13	8 (N = 2 no data)	1–20
N of SLD per patient	-	-	7	2–18
N of ctDNA or cfDNA data per patient	-	-	3	1–4

eGFR, estimated glomerular filtration rate; AST, aspartate aminotransferase; ALT, alanine aminotransferase; ALP, alkaline phosphatase; ctDNA, circulating tumor DNA; cfDNA, circulating free DNA; SLD, sum of longest diameters.

(Q/F) (40%), indicating acceptable estimation precision. High estimates for IIV on Q/F and absorption rate constant (Ka) were observed (coefficient of variation (CV%) > 100 %), with shrinkages < 30%. The parameter estimates were also in good agreement with the bootstrap results (**Table 4.2**).

The GOF plots of the final PK model demonstrated a good concordance between the model predictions and observations (**Figure S4.3**). The conditional weighted residual errors (CWRES) randomly distributed around zero without obvious trends over population predictions, but with a slight trend over time between 6–8h after last drug intake. The VPC plot (**Figure 4.2**) shows that the observed data can be adequately predicted by the developed model. Additionally, 100% of the model predicted AUC and 82.4% of the model predicted trough concentrations were within 80–120% of their corresponding observations.

Table 4.2: Parameter estimates of the population pharmacokinetic model

Parameters	Explanation	Estimate (RSE%)	IIV (CV%) (RSE%) [shrinkage%]	Bootstrap	
				Median	95% CI
CL/F (L/h)	Apparent clearance	4.10 (5%)	15.7% (31%) [48%]	4.09	3.68– 4.47
Vc/F (L)	Apparent distribution volume of the central compartment	142 (7%)	20.3% (31%) [43%]	142	125– 162
Vp/F (L)	Apparent distribution volume of the peripheral compartment	2420 (12%)	-	2462	1768– 8043
Q/F (L/h)	Apparent distribution clearance	0.548 (40%)	194.4% (15%) [28%]	0.542	0.188–1.24
Ka (/h)	Absorption rate constant	1.61 (23%)	124.5% (15%) [18%]	1.68	1.03–2.65
T_{lag} (h)	Absorption lag time	0.400 (5%)	-	0.400	0.358– 0.428
F	Bioavailability	1 fixed	16.3% (31%) [37%]	1 fixed	-
Residual errors					
Prop. Err. (CV%)	proportional residual error	15.4 (6%)	[10%]*	15.3	-
Add. Err. (SD, ng/ml)	additive residual error	44.5 (25%)	[10%]*	43.4	-

RSE, relative standard error; IIV, inter-individual variability; CI, confidence interval; CV, coefficient of variation; SD, standard deviation.
* Epsilon shrinkage.

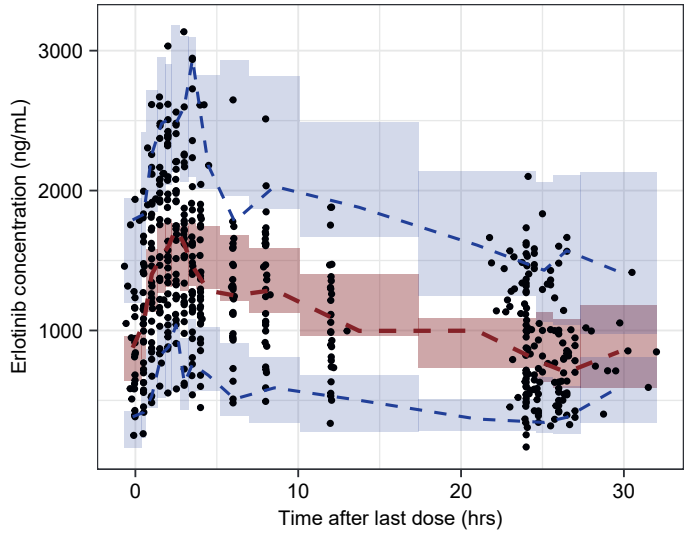

Figure 4.2: Visual predictive check (VPC) of the developed population PK model. Blue dashed lines represent 95th and 5th percentiles of the observations, red dashed line represents the 50th percentile of the observations, blue shaded areas represent 95% confidence interval of the 95th and 5th percentiles based on the simulations respectively, and red shaded area represents 95% confidence interval of the 50th percentile based on the simulations.

3.3 Tumor dynamics model

The tumor dynamics modeling results showed that the model accounting for acquired resistance only could adequately fit the data. The model that assumed the presence of primary resistance did not show an improved fit to the available data ($p > 0.05$, OFV decreased by 0.731 and AIC increased by 1.269, degree of freedom = 1). The typical estimate of T_{R_0} in this model was 4.51 mm which account for a small proportion (5.9%) of the median baseline tumor size (**Table S4.1**). Therefore, the pre-exiting resistance component was ultimately not included in the model. Furthermore, the OFV and AIC of the model incorporating an exposure-dependent decay increased by 1.441 compared with the base model, indicating no improvement in the model fit. Therefore, the exposure-dependent drug effect was not included in the final model.

The parameter estimates of the final tumor dynamics model are shown in **Table 4.3** (model code in **Supplementary Material S4.2**). The RSEs of the parameter estimates were all < 30%, indicating acceptable estimation precision. High estimates for IIV of the estimated tumor dynamics parameters were observed (CV% > 60 %). The GOF plots demonstrated a sufficient fit of the developed model to the data (**Figure S4.4**). The VPC considering the censoring of data due to progression showed that the model predicted intervals adequately captured the distribution of observations (**Figure 4.3**).

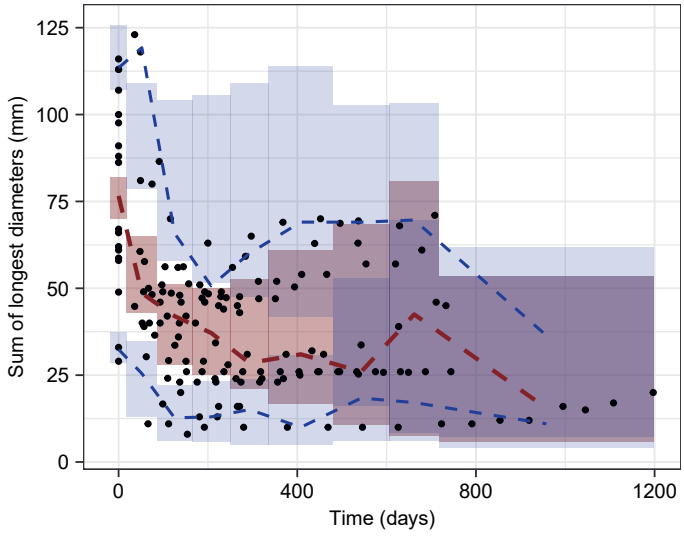

Figure 4.3: Visual predictive check (VPC) considering drop out of the developed tumor dynamics model. Blue dashed lines represent 95th and 5th percentiles of the observations, red dashed line represents the 50th percentile of the observations, blue shaded areas represent 95% confidence interval of the 95th and 5th percentiles based on the simulations respectively, and red shaded area represents 95% confidence interval of the 50th percentile based on the simulations.

Table 4.3: Parameter estimates of the tumor dynamics models without or with baseline ctDNA data incorporated

		Model without covariate		Model with baseline ctDNA data as a covariate	
Parameters	Description	Estimate (RSE%)	IIV (CV%) (RSE%) [shrinkage%]	Estimate (RSE%)	IIV (CV%) (RSE%) [shrinkage%]
k_g (/day)	Tumor growth rate constant	0.000799 (13%)	60.3% (27%) [26%]	0.00204 (25%)	16.6% (152%) [57%]
f_1	k_g change fraction when mutant EGFR VAF < 1.74%	-	-	0.334 (28%)	-
f_2	k_g change fraction when baseline ctDNA data was unavailable	-	-	0.281 (28%)	-
k_d (/day)	Tumor decay rate constant	0.0121 (19%)	68.4% (26%) [8%]	0.0123 (18%)	66.2% (22%) [7%]
k_m (/day)	Mutation rate constant	0.00911 (2%)	56.5% (25%) [19%]	0.00824 (18%)	57.9% (32%) [15%]
T_{S_0} (mm)	Baseline size of sensitive clonal population	Observed baseline	-	Observed baseline	-
T_{R_0} (mm)	Baseline size of resistant clonal population	0 fixed	-	0 fixed	-
Residual errors					
Prop. Err. (CV%)	Proportional residual error	7.54% (13%)	[12%]*	7.67% (14%)	[12%]*
Add. Err. (SD, mm)	Additive residual error	1.17 (38%)	[12%]*	1.13 (9%)	[12%]*

RSE, relative standard error; IIV, inter-individual variability; CV, coefficient of variation; SD, standard deviation, VAF, variant allele frequency.
* Epsilon shrinkage.

3.4 Genetic biomarkers and tumor dynamics

The baseline results regarding ctDNA measurements and cfDNA concentrations were available from 12 out of 18 patients and missing for 6 patients. No correlation was observed between baseline mutant *EGFR* VAF and cfDNA concentrations. According to the exploratory plots, patients with baseline mutant *EGFR* VAF ≥ 1.74% had relatively high k_g and k_m estimates, and slightly higher k_d estimates than patients with mutant *EGFR* VAF < 1.74% (**Figure 4.4**). In addition, for patients with a *TP53* mutation at baseline, the k_g and k_m estimates were relatively high compared to patients without *TP53* mutations, and comparable k_d estimates were observed (**Figure 4.4**). The association between baseline cfDNA concentrations and tumor dynamics parameters is shown in **Figure S4.5**. Patients with baseline cfDNA concentration ≥ 1.44 ng/μL showed to have higher k_g and lower k_d

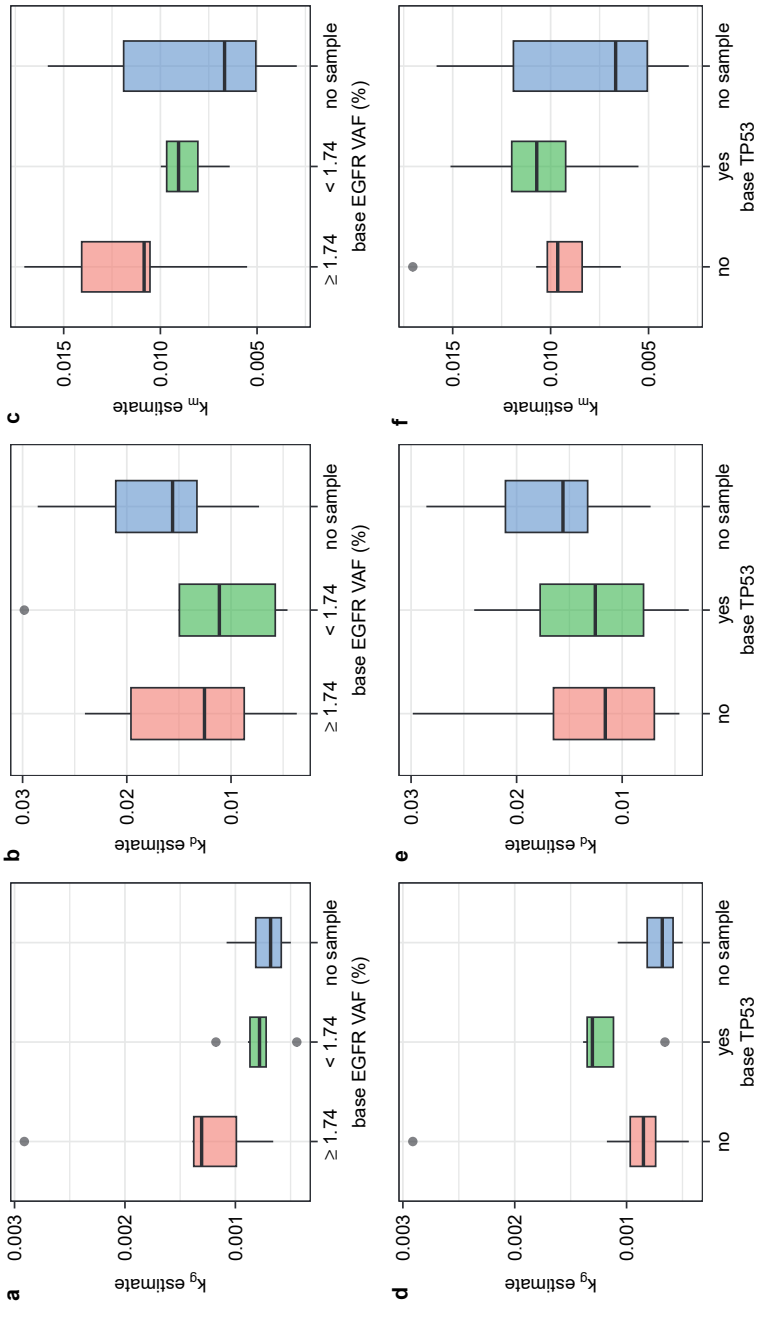

Figure 4.4: Parameter estimates from the tumor dynamics model versus baseline plasma circulating tumor DNA (ctDNA) measurements on primary mutant *EGFR* variant allele frequency and *TP53* mutation.

estimate than patients with baseline cfDNA concentration < 1.44 ng/μL, and comparable k_m estimates were observed.

When exploring the covariate effect of the baseline genetic biomarkers in the tumor dynamics model, the correlation between baseline mutant *EGFR* VAF and k_g was identified to be most significant when assigning the missing values as a separate category (OFV decreased by 11.6, $p < 0.01$, degree of freedom = 2). This correlation remained to be significant when removing the data of patients with missing covariate from the dataset (OFV decreased by 4.6, $p < 0.05$ degree of freedom = 1). The differences in k_m or k_d among patient groups with different baseline mutant *EGFR* VAF levels were shown to be not significant. Additionally, the correlations between the presence of a *TP53* mutation and tumor dynamics parameters were also not significant in the covariate analysis. The parameter estimates of the model with baseline mutant *EGFR* VAF as the covariate are shown in **Table 4.3**. The typical kg estimate in patients with baseline *EGFR* VAF ≥ 1.74% was 0.00204 day^{-1}, which is higher than the estimate for the whole population (0.000799 day^{-1}). The typical k_g estimate in patients with baseline *EGFR* VAF < 1.74% was 33.4% of that in patients with baseline *EGFR* VAF ≥ 1.74%, while the difference between patients with baseline *EGFR* VAF < 1.74% and with unknown mutant *EGFR* level was not significant. The inclusion of mutant *EGFR* VAF in the model decreased the CV% of IIV in k_g from 60.3% to 16.6%, while the corresponding RSE increased. The population predictions of the model also improved according to the GOF plots (**Figure S4.6**).

4. Discussion

In this study, the tumor dynamics and the development of drug resistance in NSCLC patients undergoing erlotinib treatment was characterized with a mathematical model accounting for tumor heterogeneity. Incorporating the erlotinib exposure into the model was also explored. The potential correlation between baseline genetic biomarkers and parameters that characterize tumor dynamics was identified with exploratory plots and confirmed with the model.

To facilitate the investigation on the exposure-tumor inhibition relationship, a population PK model of erlotinib was first developed. The estimated clearance is comparable to what has been reported previously (4.10 L/h vs 3.64–4.71 L/h) [16-19]. Due to lack of data, previously reported covariates on erlotinib PK, including the smoking status, co-medications, and alpha-1-acid glycoprotein, could not be investigated in our analysis [16, 19]. The CV% of IIV in Ka and Q/F was estimated to exceed 100%. For Ka, this high IIV estimate might

because it covers the variability in the lag time of absorption. Considering the amount of available data, these IIV estimates may not be precise. However, this does not affect the predictive ability of the PK model for the intended use in this study. The performance of the model were confirmed by the model evaluation results. However, a trend in CWRES over time between 6–8h after last drug intake was observed. This is considered to be due to the double peaks that were observed in the obtained data: data from 18 out of 29 patients who provided intensively sampled PK data demonstrate increased drug concentrations at 6-8 hours. The possible explanation could be the delayed disintegration of the tablets, food intake [20, 21], or possible enterohepatic circulation, although the latter has not been reported in literature before. This observed double peaks could not be captured by the current PK model, nor by a model considering dual first-order absorption with different lag times. Nevertheless, the model showed to be able to adequately predict the AUC of individual concentration-time curves as well as the trough concentrations which are of interest to be linked to the tumor dynamics. Therefore, the developed PK model was considered to be valid to support our study.

For the tumor size dynamics, a model accounting for intra-tumor heterogeneity and acquired resistance showed to adequately fit the obtained data, and considering primary resistance was not favored based on the available data. This may indicate that for patients with NSCLC with an activating *EGFR* mutation, it is mainly the acquired resistance, which may be due to the acquisition of *EGFR* p.T790M mutation or other mechanisms, that limits the treatment response. Among previously reported model-based studies on tumor size dynamics in NSCLC patients undergoing erlotinib treatment, one study also considered tumor heterogeneity [22]. Their results also showed that the models with and without primary resistance could describe the data equally well even though erlotinib was used as a second-line treatment in their study [22]. However, it is worth noting that the model presented in the current study is empirical and simplifies the complex process of the emergence of treatment resistance. Previously, several mechanistic models have been proposed to provide quantitative insight into this process [23, 24]. The relatively limited amount of data in the current analysis prohibits the implementation of more mechanistic models and therefore may limit the mechanistic interpretation. In fact, the presence of *TP53* mutations may indicate the presence of primary resistance [25, 26]. However, *TP53* mutations were only detected in 4 out of 18 patients which may be unable to provide significant impact to our model. Nonetheless, this more empirical approach does take into account the existence and interaction among multiple clonal populations which are crucial for understanding resistance development [24]. We do consider this approach relevant for exploring optimal guided drug treatment in real world clinical oncology practice where

extensive data is normally sparse. Furthermore the current approach can serve as a basis for building more mechanistic-based models when more extensive data is available [24]. The growth rates of treatment sensitive and resistant clonal populations were assumed to be the same in the model. This was because of the lack of identifiability of separate growth rates due to the limited amount of data.

The current study did not identify a clear exposure-tumor inhibition relationship within the current concentration range (the median predicted drug concentrations at the tumor size monitoring time points was 992 ng/ml (range of 284–1554 ng/mL)), neither when assuming a non-linear relationship with the Emax model. A dose-tumor inhibition relationship was also explored but no clear relationship was identified. This might be because the treatment effect has already been saturated. The dose level selected for erlotinib (i.e. 150 mg daily) is the maximum tolerated dose, under which the average trough concentration at steady state is well above what is required for the required erlotinib activity and considered to be sufficient to provide a high anti-neoplastic effect [27]. This lack of relationship is in line with previous clinical studies where no significant correlation between erlotinib exposure and response has been identified [28-30]. One study also showed that increased erlotinib exposure had less impact on the antitumor effects in EGFR mutation-positive patients [31]. As an exposure-response relationship was not identified, we could not investigate the influence of drug exposure on the evolving tumor progression in this case. However, this result suggests that there is a potential option to decrease the dose of erlotinib to target for a lower concentration range that still ensures sufficient efficacy but can be better tolerated, especially since a significant proportion of erlotinib-treated patients can have severe toxicity [6]. The U.S. Food and Drug Administration (FDA) has recently proposed the Project Optimus which also encourages to improve dose selection and optimization for oncology drugs by accounting for both efficacy and tolerability rather than automatically selecting the maximum tolerated dose [32, 33]. A recent study has already suggested an optimized starting dose of 50–60 mg/day for erlotinib and a concentration range of 150–310 ng/mL for personalized erlotinib treatment in NSCLC patients considering both efficacy and tolerability [34].

The correlation between baseline genetic biomarkers and parameters in tumor dynamics model was investigated in this study. The VAF's of mutant *EGFR* and the presence of *TP53* mutations in ctDNA at baseline showed to have potential correlation with the estimated parameters in the tumor dynamics model (mainly k_g and k_m), especially that higher baseline *EGFR* VAF was significantly correlated with increased growth rate constant k_g. This indicates that patients with higher *EGFR* VAF at baseline may have a worse response to the treatment, which is in line with the clinical findings from a *EGFR* cohort in the

START-TKI study, i.e. patients without detectable ctDNA at baseline had a lower rate of radiological progression [6]. An explanation could be the association between ctDNA levels and tumor burden [11, 35]. Our result is also in line with previous findings that baseline concomitant *TP53* mutations may relate to worse clinical outcome in patients with NSCLC [6]. After incorporating baseline ctDNA measurements, the developed tumor dynamics model could better predict the tumor sizes dynamics in response to erlotinib treatment in NSCLC patients. This finding also demonstrates the potential to use baseline ctDNA as an early biomarker to support decision making for the treatment of NSCLC patients [36].

This study also has some limitations. The results found in the current study are based on limited data from a limited number of patients, especially for genetic biomarkers. The unavailability of baseline cfDNA samples in 6 out of 18 patients could also impact the interpretation of the results, as well as the determination of the threshold value of EGFR *VAF* which was associated with increased growth rates. However, this study is one of the first that investigated the relationships among PK, tumor dynamics, and ctDNA measurements. Furthermore, since the data on detectable mutation levels in ctDNA are limited, development of a model for describing longitudinal ctDNA data was not feasible and only the baseline ctDNA measurements were included in the analysis, which however explored the value of ctDNA as an early biomarker. Additionally, the mutant *EGFR* VAF was only investigated as a categorical covariate while the data range from 0% to 62.74% and correspond to multiple variants. Therefore, further analysis with more extensive data is warranted to validate the current results and to explore the correlation between the longitudinal ctDNA measurements and tumor size dynamics with models.

In conclusion, our study demonstrated that the model accounting for intra-tumor heterogeneity and acquired resistance can well characterize the tumor size dynamics in NSCLC patients during erlotinib treatment. No clear exposure-tumor inhibition relationship was identified within the current concentration range. A correlation between baseline ctDNA measurements and tumor growth rates was however identified which suggests that quantitative ctDNA measurements at baseline have potential to be predictive of anti-cancer treatment response, and further study on more extensive longitudinal data is warranted. The developed model can potentially be further applied to design optimal treatment regimens that better overcome resistance.

Study highlights

What is the current knowledge on the topic?

Insight into the evolutionary development of treatment resistance can support optimization of anti-cancer treatments. This is also the case in non-small cell lung cancer (NSCLC) patients. A model-based approach can support such study based on data on pharmacokinetics, tumor sizes and genetic biomarkers

What question did this study address?

We aimed to quantitatively characterize the tumor dynamics and evolving resistance development in NSCLC patients treated with erlotinib, and investigate the relationship between baseline circulating tumor DNA (ctDNA) measurements and tumor dynamics.

What does this study add to our knowledge?

A model accounting for intra-tumor heterogeneity and acquired resistance well characterized the tumor size dynamics in NSCLC patients during erlotinib treatment. No exposure-tumor inhibition relationship was identified in the identified exposure range. Baseline ctDNA data on mutant *EGFR* levels correlate with tumor growth rate and the inclusion of ctDNA data improved model prediction.

How might this change drug discovery, development, and/or therapeutics?

Our findings suggest that baseline ctDNA measurements have the potential to be a predictor of anti-cancer treatment response, which encouraged to use ctDNA as an early biomarker. The developed model can further be applied to design optimal treatment regimens to better overcome resistance.

References

1. Zhao B, Hemann MT, Lauffenburger DA. Modeling Tumor Clonal Evolution for Drug Combinations Design. Trends Cancer. 2016;2(3):144-58. doi:10.1016/j.trecan.2016.02.001.
2. Sun X, Hu B. Mathematical modeling and computational prediction of cancer drug resistance. Brief Bioinform. 2018;19(6):1382-99. doi:10.1093/bib/bbx065.
3. Nagano T, Tachihara M, Nishimura Y. Mechanism of Resistance to Epidermal Growth Factor Receptor-Tyrosine Kinase Inhibitors and a Potential Treatment Strategy. Cells. 2018;7(11):212. doi:10.3390/cells7110212.
4. Oliveira KCS, Ramos IB, Silva JMC, Barra WF, Riggins GJ, Palande V, et al. Current Perspectives on Circulating Tumor DNA, Precision Medicine, and Personalized Clinical Management of Cancer. Mol Cancer Res. 2020;18(4):517-28. doi:10.1158/1541-7786.MCR-19-0768.
5. Herbreteau G, Vallee A, Charpentier S, Normanno N, Hofman P, Denis MG. Circulating free tumor DNA in non-small cell lung cancer (NSCLC): clinical application and future perspectives. J Thorac Dis. 2019;11(Suppl 1):S113-S26. doi:10.21037/jtd.2018.12.18.
6. Steendam CMJ, Veerman GDM, Pruis MA, Atmodimedjo P, Paats MS, van der Leest C, et al. Plasma Predictive Features in Treating EGFR-Mutated Non-Small Cell Lung Cancer. Cancers (Basel). 2020;12(11):3179. doi:10.3390/cancers12113179.
7. Barbolosi D, Ciccolini J, Lacarelle B, Barlesi F, Andre N. Computational oncology--mathematical modelling of drug regimens for precision medicine. Nature Reviews Clinical Oncology. 2016;13(4):242-54. doi:10.1038/nrclinonc.2015.204.
8. Buil-Bruna N, Lopez-Picazo JM, Martin-Algarra S, Troconiz IF. Bringing Model-Based Prediction to Oncology Clinical Practice: A Review of Pharmacometrics Principles and Applications. Oncologist. 2016;21(2):220-32. doi:10.1634/theoncologist.2015-0322.
9. Kimko H, Pinheiro J. Model-based clinical drug development in the past, present and future: a commentary. Br J Clin Pharmacol. 2015;79(1):108-16. doi:10.1111/bcp.12341.
10. Yin A, van Hasselt JGC, Guchelaar HJ, Friberg LE, Moes D. Anti-cancer treatment schedule optimization based on tumor dynamics modelling incorporating evolving resistance. Sci Rep. 2022;12(1):4206. doi:10.1038/s41598-022-08012-7.
11. Wan JCM, Massie C, Garcia-Corbacho J, Mouliere F, Brenton JD, Caldas C, et al. Liquid biopsies come of age: towards implementation of circulating tumour DNA. Nat Rev Cancer. 2017;17(4):223-38. doi:10.1038/nrc.2017.7.
12. Janssen JM, Verheijen RB, van Duijl TT, Lin L, van den Heuvel MM, Beijnen JH, et al. Longitudinal nonlinear mixed effects modeling of EGFR mutations in ctDNA as predictor of disease progression in treatment of EGFR-mutant non-small cell lung cancer. Clin Transl Sci. 2022;15(8):1916-25. doi:10.1111/cts.13300.
13. van Leeuwen RW, Peric R, Hussaarts KG, Kienhuis E, NS IJ, de Bruijn P, et al. Influence of the Acidic Beverage Cola on the Absorption of Erlotinib in Patients With Non-Small-Cell Lung Cancer. J Clin Oncol. 2016;34(12):1309-14. doi:10.1200/JCO.2015.65.2560.
14. Veerman GDM, Hussaarts K, Peric R, Oomen-de Hoop E, Landa KD, van der Leest CH, et al. Influence of Cow's Milk and Esomeprazole on the Absorption of Erlotinib: A Randomized, Crossover Pharmacokinetic Study in Lung Cancer Patients. Clin Pharmacokinet. 2021;60(1):69-77. doi:10.1007/s40262-020-00910-1.
15. Eisenhauer EA, Therasse P, Bogaerts J, Schwartz LH, Sargent D, Ford R, et al. New response evaluation criteria in solid tumours: revised RECIST guideline (version 1.1). Eur J Cancer. 2009;45(2):228-47. doi:10.1016/j.ejca.2008.10.026.
16. Emoto-Yamamoto Y, Iida S, Kawanishi T, Fukuoka M. Population pharmacokinetics of erlotinib in Japanese patients with advanced non-small cell lung cancer. J Clin Pharm Ther. 2015;40(2):232-9. doi:10.1111/jcpt.12232.

17. Parra-Guillen ZP, Berger PB, Haschke M, Donzelli M, Winogradova D, Pfister B, et al. Role of Cytochrome P450 3A4 and 1A2 Phenotyping in Patients with Advanced Non-small-Cell Lung Cancer Receiving Erlotinib Treatment. Basic Clin Pharmacol Toxicol. 2017;121(4):309-15. doi:10.1111/bcpt.12801.
18. Endo-Tsukude C, Sasaki JI, Saeki S, Iwamoto N, Inaba M, Ushijima S, et al. Population Pharmacokinetics and Adverse Events of Erlotinib in Japanese Patients with Non-small-cell Lung Cancer: Impact of Genetic Polymorphisms in Metabolizing Enzymes and Transporters. Biol Pharm Bull. 2018;41(1):47-56. doi:10.1248/bpb.b17-00521.
19. Evelina C, Guidi M, Khoudour N, Pascaline B-R, Fabre E, Tlemsani C, et al. Population Pharmacokinetics of Erlotinib in Patients With Non-small Cell Lung Cancer: Its Application for Individualized Dosing Regimens in Older Patients. Clin Ther. 2020;42(7):1302-16. doi:10.1016/j.clinthera.2020.05.008.
20. Rampaka R, Ommi K, Chella N. Role of solid lipid nanoparticles as drug delivery vehicles on the pharmacokinetic variability of Erlotinib HCl. Journal of Drug Delivery Science and Technology. 2021;66:102886. doi:https://doi.org/10.1016/j.jddst.2021.102886.
21. Veerman GDM, Hussaarts K, Jansman FGA, Koolen SWL, van Leeuwen RWF, Mathijssen RHJ. Clinical implications of food-drug interactions with small-molecule kinase inhibitors. Lancet Oncol. 2020;21(5):e265-e79. doi:10.1016/S1470-2045(20)30069-3.
22. Mistry HB, Helmlinger G, Al-Huniti N, Vishwanathan K, Yates J. Resistance models to EGFR inhibition and chemotherapy in non-small cell lung cancer via analysis of tumour size dynamics. Cancer Chemother Pharmacol. 2019;84(1):51-60. doi:10.1007/s00280-019-03840-3.
23. Foo J, Michor F. Evolution of acquired resistance to anti-cancer therapy. Journal of theoretical biology. 2014;355:10-20. doi:10.1016/j.jtbi.2014.02.025.
24. Terranova N, Girard P, Klinkhardt U, Munafo A. Resistance Development: A Major Piece in the Jigsaw Puzzle of Tumor Size Modeling. CPT Pharmacometrics Syst Pharmacol. 2015;4(6):320-3. doi:10.1002/psp4.45.
25. Canale M, Petracci E, Delmonte A, Chiadini E, Dazzi C, Papi M, et al. Impact of TP53 Mutations on Outcome in EGFR-Mutated Patients Treated with First-Line Tyrosine Kinase Inhibitors. Clin Cancer Res. 2017;23(9):2195-202. doi:10.1158/1078-0432.Ccr-16-0966.
26. Ulivi P, Delmonte A, Chiadini E, Calistri D, Papi M, Mariotti M, et al. Gene mutation analysis in EGFR wild type NSCLC responsive to erlotinib: are there features to guide patient selection? Int J Mol Sci. 2014;16(1):747-57. doi:10.3390/ijms16010747.
27. US Food and Drug Administration. Drug approval package: Tarceva (Erlotinib) Tablets (Application No.: 021743). https://www.accessdata.fda.gov/drugsatfda_docs/nda/2004/21-743_Tarceva.cfm.
28. Yu H, Steeghs N, Nijenhuis CM, Schellens JH, Beijnen JH, Huitema AD. Practical guidelines for therapeutic drug monitoring of anticancer tyrosine kinase inhibitors: focus on the pharmacokinetic targets. Clin Pharmacokinet. 2014;53(4):305-25. doi:10.1007/s40262-014-0137-2.
29. Verheijen RB, Yu H, Schellens JHM, Beijnen JH, Steeghs N, Huitema ADR. Practical Recommendations for Therapeutic Drug Monitoring of Kinase Inhibitors in Oncology. Clin Pharmacol Ther. 2017;102(5):765-76. doi:10.1002/cpt.787.
30. Kenmotsu H, Imamura CK, Kawamura T, Oyakawa T, Omori S, Nakashima K, et al. Prospective evaluation of the relationship between response and exposure of total and unbound erlotinib in non-small cell lung cancer patients. Cancer Chemother Pharmacol. 2022;90(2):115-23. doi:10.1007/s00280-022-04452-0.

31. Fukudo M, Ikemi Y, Togashi Y, Masago K, Kim YH, Mio T, et al. Population pharmacokinetics/pharmacodynamics of erlotinib and pharmacogenomic analysis of plasma and cerebrospinal fluid drug concentrations in Japanese patients with non-small cell lung cancer. Clin Pharmacokinet. 2013;52(7):593-609. doi:10.1007/s40262-013-0058-5.
32. Fourie Zirkelbach J, Shah M, Vallejo J, Cheng J, Ayyoub A, Liu J, et al. Improving Dose-Optimization Processes Used in Oncology Drug Development to Minimize Toxicity and Maximize Benefit to Patients. J Clin Oncol. 2022;40(30):3489-500. doi:10.1200/JCO.22.00371.
33. Shah M, Rahman A, Theoret MR, Pazdur R. The Drug-Dosing Conundrum in Oncology - When Less Is More. N Engl J Med. 2021;385(16):1445-7. doi:10.1056/NEJMp2109826.
34. Takeda Y, Ishizuka N, Sano K, Hirano S, Suzuki M, Naka G, et al. Phase I/II Study of Erlotinib to Determine the Optimal Dose in Patients With Non-Small Cell Lung Cancer Harboring Only EGFR Mutations. Clin Transl Sci. 2020;13(6):1150-60. doi:10.1111/cts.12796.
35. Sanz-Garcia E, Zhao E, Bratman SV, Siu LL. Monitoring and adapting cancer treatment using circulating tumor DNA kinetics: Current research, opportunities, and challenges. Sci Adv. 2022;8(4):eabi8618. doi:10.1126/sciadv.abi8618.
36. Bruno R, Chanu P, Kagedal M, Mercier F, Yoshida K, Guedj J, et al. Support to early clinical decisions in drug development and personalised medicine with checkpoint inhibitors using dynamic biomarker-overall survival models. British journal of cancer. 2023. doi:10.1038/s41416-023-02190-5.

Supplementary Material S4.1

Population PK analysis - covariate analysis methods

In the population PK analysis, patients' demographic information, including age, sex, weight, height, and laboratory test results, including creatinine, estimated glomerular filtration rate (eGFR), albumin, total bilirubin, aspartate aminotransferase (AST), alanine aminotransferase (ALT), and alkaline phosphatase (ALP) were investigated as covariates. The stepwise covariate modeling (SCM) function of Perl-speaks NONMEM (version 4.9) was applied to perform the covariate analysis. The effect of all covariates on erlotinib clearance and that of weight, height, and albumin on apparent distribution volume of the central compartment were investigated. Model selection was based on the reduction in objective function value (OFV) (a likelihood ratio test) assuming a χ^2 distribution, a reduction in IIV, and physiological plausibility. The *p* values were set as 0.05 and 0.01 for the forward selection and backward elimination process, respectively.

The effects of continuous covariates were investigated with both linear relation (Eq. S4.1) and power relation (Eq. S4.2), where P_i represents the parameter of *i*th individual, P_t represents typical value of the parameter, and η_i represents the individual variability, θ_{COV} represents the estimate of covariate effect, COV_i represents the covariate value of *i*th individual, COV_m is the median value of the covariate. Categorical covariates (e.g. sex) were analyzed with Eq. S4.3, where θ_{COV} was set as 1 for reference category (e.g. males) and was estimated for other categories (e.g. females).

$$P_i = P_t \cdot (1 \pm \theta_{COV} \cdot (COV_i - COV_m)) \cdot e^{\eta_i} \quad \text{Eq. S4.1}$$

$$P_i = P_t \cdot \left(\frac{COV_i}{COV_m}\right)^{\theta_{COV}} \cdot e^{\eta_i} \quad \text{Eq. S4.2}$$

$$P_i = P_t \cdot \theta_{COV} \cdot e^{\eta_i} \quad \text{Eq. S4.3}$$

Supplementary Material S4.2

NONMEM code for the tumor dynamics model

```
$INPUT
C ID DROP TIME TAD AMT ADDL II CMT EVID DV
UNDERTREAT; if treatment started: 1, yes
DROP DROP Dose; dose
DROP AGE SEX HT WT DROP BMI
baseTS;  baseline tumor size
T790M; T790M: 1, yes
TP53_base; presence of TP53: 1, yes
basecfDNA; baseline cfDNA concentration
baseVAF; baseline EGFR mutant levels
DROP DROP DROP DROP DROP DROP DROP
ICL IV2 IV3 IQ IKA IALAG1 IF1; individual PK parameters

$DATA START_all6.csv IGNORE=C IGNORE=(CMT.GT.4) IGNORE=(CMT.EQ.2); only
data of tumor sizes

$SUBROUTINES ADVAN13 TOL=4

$MODEL
COMP = (DEPOT)
COMP = (CENTRAL,DEFOBS)
COMP = (PRIPH)
COMP = (TUMOR)
COMP = (TUMOR2)

$PK
KG1 = THETA(1)* EXP(ETA(1))/100
KD1 = THETA(2)* EXP(ETA(2))/100
KM1 = THETA(5)* EXP(ETA(3))/100
;IF(baseVAF.GE.0.AND.baseVAF.LT.1.74) KG1=THETA(6)*KG1
;IF(baseVAF.LT.0) KG1=THETA(7)*KG1; no sample group

CL = ICL*24; change unit from L/h to L/day
V2 = IV2
V3 = IV3
```

```
Q = IQ *24
ALAG1 = IALAG1 /24
KA = IKA*24
F1 = IF1
K=CL/V2
K23=Q/V2
K32=Q/V3

BASES = baseTS
A_0(4)=BASES
A_0(5)=0

$DES
DADT(1) = -KA*A(1); can simulate drug concentrations, if needed
DADT(2)= KA*A(1) - K*A(2) -K23*A(2) +K32*A(3); can simulate drug concentrations,
if needed
DADT(3) = K23*A(2)- K32*A(3); can simulate drug concentrations, if needed
DADT(4) = KG1*A(4)-KD1* UNDERTREAT *A(4) - KM1* UNDERTREAT *A(4)
DADT(5) = KM1* UNDERTREAT *A(4)+ KG1* UNDERTREAT *A(5)

$ERROR
TS=A(4)+A(5)
IPRED = TS
   W = SQRT(THETA(3)**2*IPRED**2 + THETA(4)**2)
   Y = IPRED + W*EPS(1)
 IRES = DV-IPRED
IWRES = IRES/W

$THETA
(0.001,0.1,1); KG1
(0.1,1,5); KD
(0.01,0.1,1); Prop err
(0.1,1,10); Add err
(0.01,1, 5); KM1
;(0.05,0.5,2); VAF < 1.74
;(0.05,0.5,2); VAF not available

$OMEGA
0.1; IIV KG
```

```
0.1; IIV KD
0.1; IIV KM1

$SIGMA  1  FIX;
$ESTIMATION METHOD=1 INTER MAXEVAL=9999 NOABORT SIG=3 PRINT=10
POSTHOC
$COV print=E

$TABLE ID TIME TAD MDV EVID UNDERTREAT Dose baseTS T790M TP53_base
basecfDNA baseVAF baseTS KG1 KD1 KM1 TS IPRED IW
```

Supplementary figures and table

Supplementary Figures

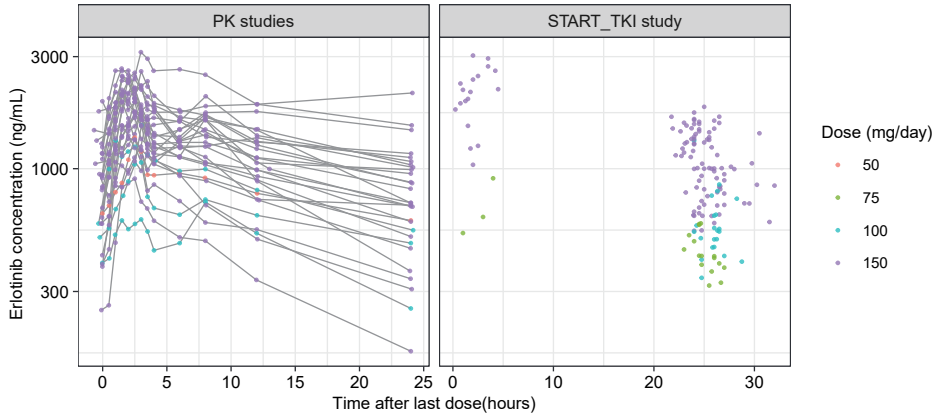

Figure S4.1: The collected data on erlotinib concentrations over time.

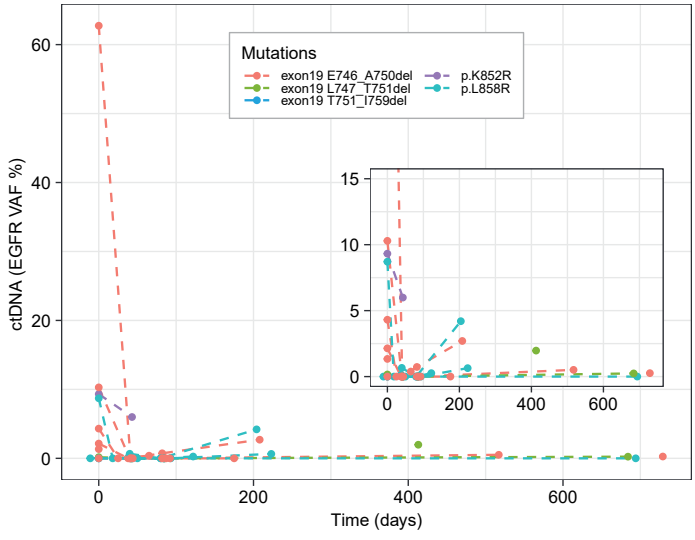

Figure S4.2: The collected variant allele frequency of primary EGFR variants detected from circulating free DNA (cfDNA) (ctDNA data) over time.

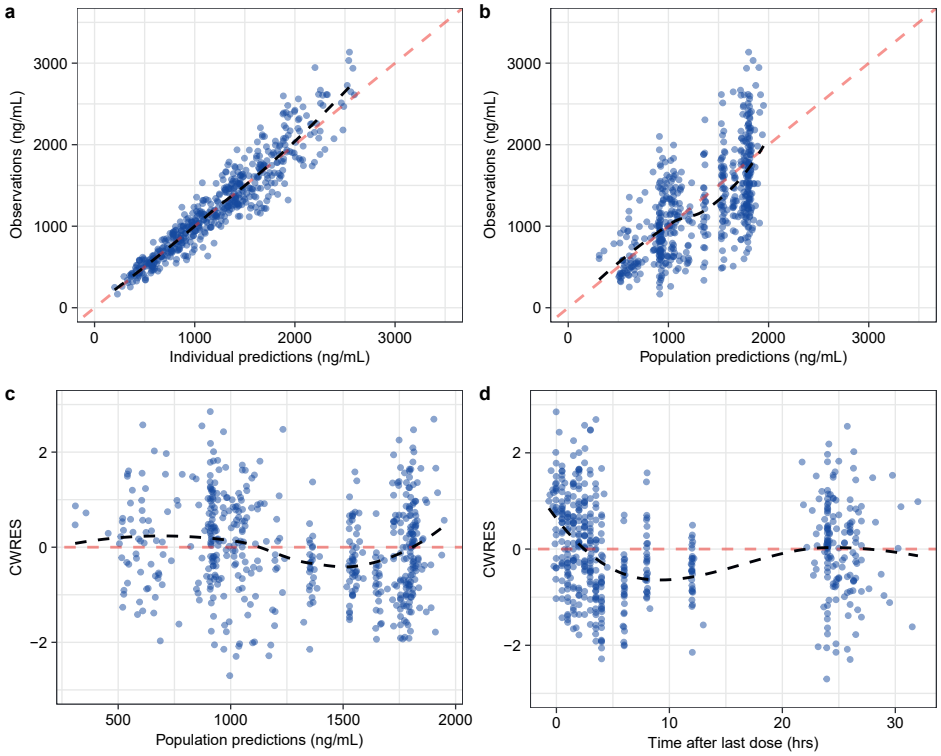

Figure S4.3: Goodness-of-fit plots of the developed population PK model, including observations versus individual predictions (a) and population predictions (b), and conditional weighted residual errors (CWRES) versus populations predictions (c) and versus time after last dose (d). The red dashed lines represent y = x (a, b) and y = 0 (c, d). Black dashed lines represent corresponding loess regressions.

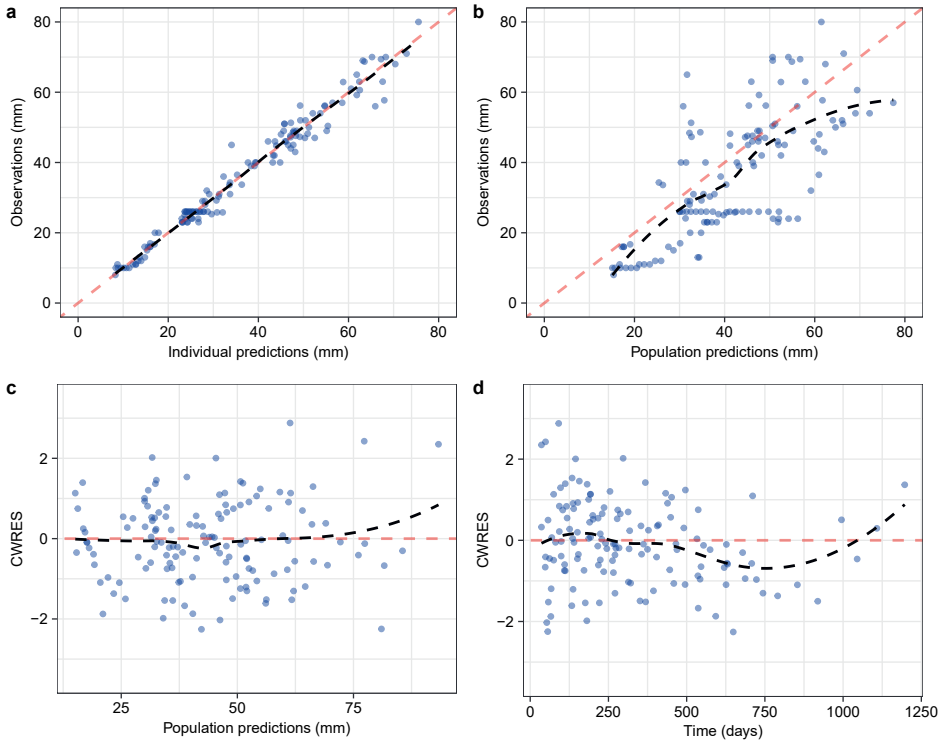

Figure S4.4: Goodness-of-fit plots of the developed tumor dynamics model, including observations versus individual predictions (a) and population predictions (b), and conditional weighted residual errors (CWRES) versus populations predictions (c) and versus time (d). The red dashed lines represent y = x (a, b) and y = 0 (c, d). Black dashed lines represent corresponding loess regressions.

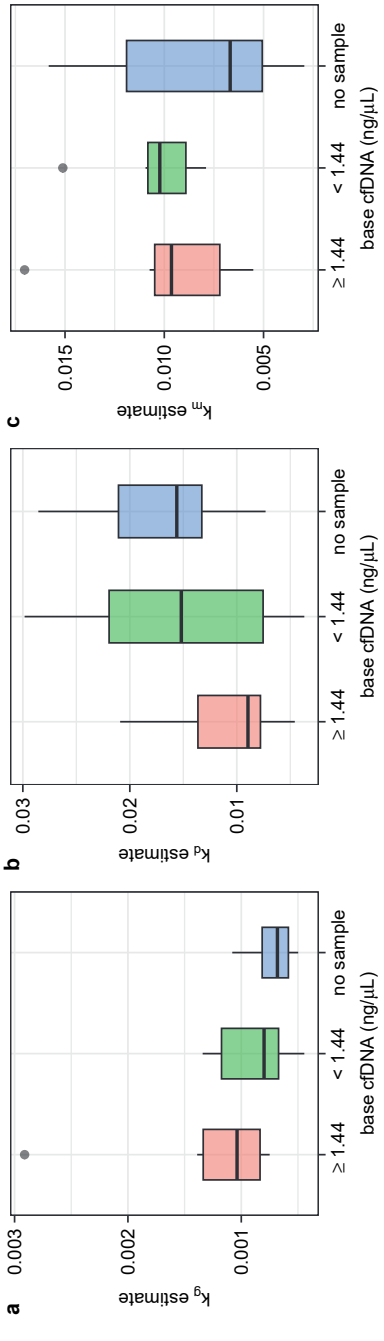

Figure S4.5: Parameter estimates from the tumor dynamics model versus baseline circulating free DNA (cfDNA) concentrations.

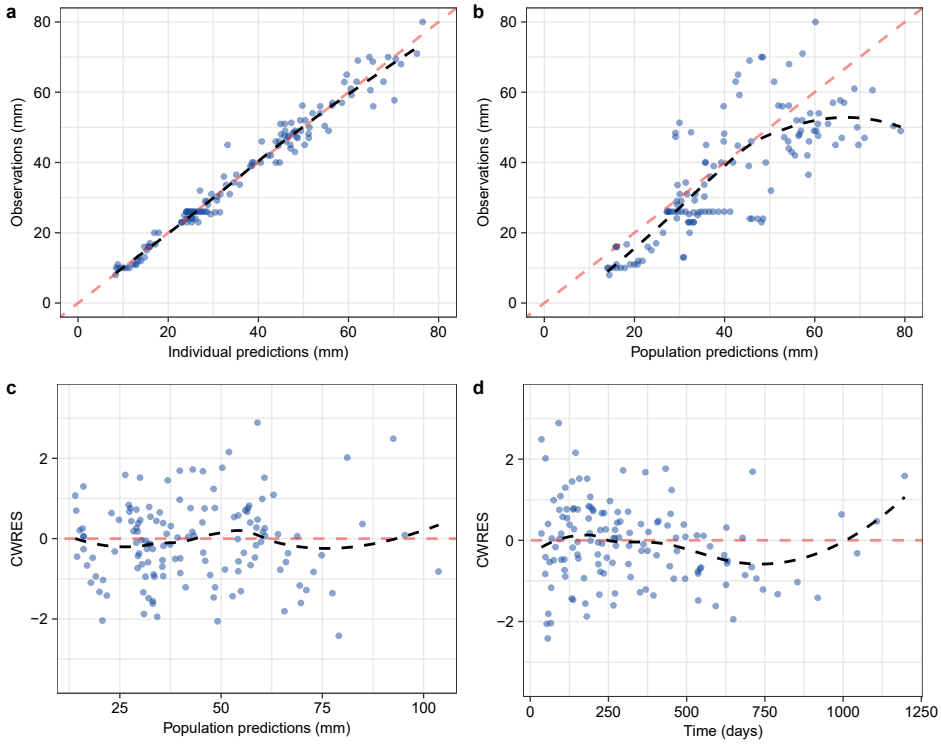

Figure S4.6: Goodness-of-fit plots of the tumor dynamics model with ctDNA as a covariate, including observations versus individual predictions (a) and population predictions (b), and conditional weighted residual errors (CWRES) versus populations predictions (c) and versus time (d). The red dashed lines represent y = x (a, b) and y = 0 (c, d). Black dashed lines represent corresponding loess regressions.

Supplementary Table

Table S4.1: Parameter estimates of the tumor dynamics model considering pre-existing resistance component (primary resistance)

Parameters	Description	Estimate (RSE%)	IIV (CV%) (RSE%) [shrinkage%]
k_g (/day)	Tumor growth rate constant	0.000801 (22%)	60.4% (29%) [26%]
k_d (/day)	Tumor decay rate constant	0.0129 (21%)	73.6% (27%) [8%]
k_m (/day)	Mutation rate constant	0.00756 (28%)	66.6% (34%) [19%]
T_{S_0} (mm)	Baseline size of sensitive clonal population	Observed baseline - T_{R_0}	-
T_{R_0} (mm)	Baseline size of resistant clonal population	4.51 (39%)	0 fixed
Residual errors			
Prop. Err. (CV%)	Proportional residual error	7.44% (18%)	[12%]*
Add. Err. (SD, mm)	Additive residual error	1.19 (21%)	[12%]*